Domain decomposition methods for a three dimensional extrusion model

Merete S. Eikemo [1] and Magne S. Espedal [2]

Abstract. An extrusion process in three dimensions is modelled, and gives rise to indefinite block systems. The multi-scaled complex geometry involved in such a process is one of the main motivations for making use of domain decomposition methods for this problem. An overlapping additive Schwarz method will be used, which allows the possibility of local refinement at locations where the system experiences large gradients. For a nonlinear parabolic equation an alternating Schwarz method will be presented.

INTRODUCTION

The thermo-mechanical properties of aluminium during an extrusion process is described by a coupled set of nonlinear partial differential equations. The model consists of a temperature equation, a continuity equation and Navier-Stokes equations with a nonlinear Zener-Holloman material law for velocities and pressure. In order to support practical applications and being able to take into account the behaviour of the aluminium as it flows through the complex geometry of a die, the model has to be three dimensional.

The first three sections will briefly introduce an aluminium process, present the

[1] Department. of Mathematics, University of Bergen, Johs. Brunsgt.12, 5008 Bergen, Norway, merete.eikemo@mi.uib.no

[2] Department. of Mathematics, University of Bergen, Johs. Brunsgt.12, 5008 Bergen, Norway, resme@mi.uib.no

Domain Decomposition Methods in Sciences and Engineering, edited by R. Glowinski *et al.*

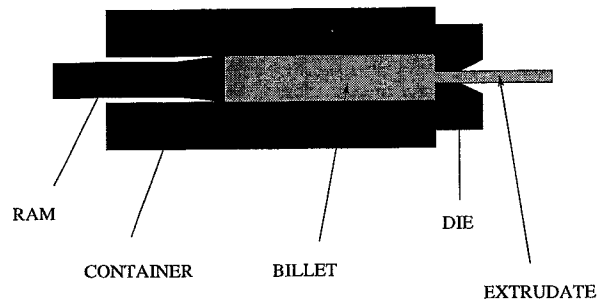

Figure 1 Aluminium extrusion process.

model equations and describe the solution procedure. The domain decomposition ideas for the model and some numerical results will be given in the last two sections.

ALUMINIUM EXTRUSION PROCESS

A preheated aluminium billet is placed in a container. The typical initial temperature is 450°C and the length of the billet is half a meter. At one end a die is placed, and as a result of a slowly moving ram in the other end and the shape of the die, the billet is deformed into a complex thin-walled profile of specified design, [HSH92]. Figure 1 gives a schematic picture of such an extrusion process with a simple die shape.

MODEL

The governing nonlinear equations are the pressure-velocity equations

$$\begin{aligned} \mathrm{Re}(\frac{\partial \mathbf{u}}{\partial t} + \mathbf{u} \cdot \nabla \mathbf{u}) &= -\nabla p + \nabla \cdot \tau \qquad \text{in } \Omega, \\ \nabla \cdot \mathbf{u} &= 0 \qquad \text{in } \Omega, \end{aligned} \tag{1}$$

together with the heat balance equation

$$\mathrm{Pe}(\frac{\partial \theta}{\partial t} + \mathbf{u} \cdot \nabla \theta) = \nabla^2 \theta + \beta \epsilon : \tau \quad \text{in } \Omega, \tag{2}$$

where Ω is the physical domain where the extrusion process takes place. The primary variables are the velocity $\mathbf{u}$, the pressure p and the temperature θ. Further, $\tau = 2\mu\epsilon$ is the stress tensor, where $\mu = \bar{\tau}/(3\bar{\epsilon})$ is the nonlinear viscosity coeffisient. Here $\bar{\tau}(\bar{\epsilon}, \theta) = \alpha^{-1}\mathrm{arcsinh}((Z/K)^{\frac{1}{m}})$ is the Zener-Holloman material model with the parameter $Z = Z(\bar{\epsilon}, \theta) = \bar{\epsilon}\exp(Q/(R\theta))$. The viscosity coeffisient also consists of the effective strain rate $\bar{\epsilon} = (\frac{2}{3}\epsilon : \epsilon)^{\frac{1}{2}}$, where $\epsilon = \frac{1}{2}(\nabla \mathbf{u} + \nabla \mathbf{u}^t)$ is the strain rate tensor. The parameters α, m, K, Q, R and β are problem- and material dependent with typical values [Sæv93]. The Reynolds number and the Péclét number are, in the equations, denoted by Re and Pe, respectively.

From specific material- and problem-dependent parameters we get the Reynolds number to be very small, typical of magnitude 10^{-8}. We may therefore neglect the left side of the vector equation in (1), but note that the equation still is strongly nonlinear because of the term $\nabla \cdot \tau$.

$$\begin{aligned} -\nabla \cdot \tau + \nabla p &= 0 \qquad \text{in } \Omega, \\ \nabla \cdot \mathbf{u} &= 0 \qquad \text{in } \Omega. \end{aligned} \tag{3}$$

SOLUTION PROCEDURE

The pressure and velocity are slowly varying over a timestep relative the variation of the temperature. To decouple the heat balance equation from the other equations, we therefore, on each timelevel, use a sequential iterative solution procedure. In the first step the pressure-velocity system (3) is solved, using the temperature solution from the previous timestep. In the second step the temperature equation (2) is solved, using the velocity from the first step. The further iterations between these two steps are performed using the most recently calculated temperature for the solving of the pressure-velocity system. Each equation is linearized by Picard iterations.

The discretization is done by using a mixed finite element approch with hexahedral elements and a triquadratic approximation for velocity and trilinear approximation for pressure and temperature. Carried out on (3), this results in a linear block system of the form

$$\begin{Bmatrix} A_{11} & A_{12} & A_{13} & B_1^t \\ A_{21} & A_{22} & A_{23} & B_2^t \\ A_{31} & A_{32} & A_{33} & B_3^t \\ B_1 & B_2 & B_3 & 0 \end{Bmatrix} \begin{Bmatrix} X \\ Y \end{Bmatrix} = \begin{Bmatrix} A & B^t \\ B & 0 \end{Bmatrix} \begin{Bmatrix} X \\ Y \end{Bmatrix} = \begin{Bmatrix} F \\ G \end{Bmatrix}, \tag{4}$$

where B^t is the transpose of B. Bramble and Pasciak, [BP94], give a method for solving systems of this kind. The system (4) is reformulated in such a way that the new coeffisient matrix $\tilde{M}$ is positive definite,

$$\tilde{M} \begin{Bmatrix} X \\ Y \end{Bmatrix} = \begin{Bmatrix} A_0^{-1}A & A_0^{-1}B^t \\ BA_0^{-1}(A - A_0) & BA_0^{-1}B^t \end{Bmatrix} \begin{Bmatrix} X \\ Y \end{Bmatrix} = \begin{Bmatrix} A_0^{-1}F \\ BA_0^{-1}F - G \end{Bmatrix}. \tag{5}$$

Here A_0 is a preconditioner for A.

Let

$$\tilde{M}_0 = \begin{Bmatrix} I & 0 \\ 0 & \mathcal{K} \end{Bmatrix}, \tag{6}$$

where I is the identity matrix and $\mathcal{K}$ is the preconditioner for the Schur complement $BA^{-1}B^t$,

$$\mathcal{K} = N_h + h^2 I, \tag{7}$$

where N_h is the solution operator on the pressure grid for a finite element approximation to a Neumann problem and h is the spatial resolution. Each evaluation of the preconditioner $\mathcal{K}$ then requires solving a discrete Neumann problem on a grid of mesh size h. This preconditioner, [BP94], gives rise to convergence rates which can be bounded independently of h.

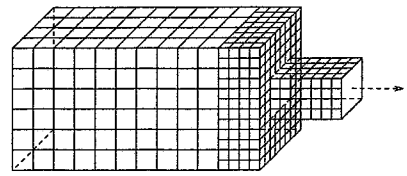

Figure 2 Full domain with refined outlet area.

A new inner product can be defined,

$$\left[\left\{\begin{array}{c} U \\ V \end{array}\right\}, \left\{\begin{array}{c} X \\ Y \end{array}\right\}\right] \equiv (AU, X) - (A_0 U, X) + (V, Y), \tag{8}$$

in which the matrix $\tilde{M}$ is symmetric. In addition to the matrix $\tilde{M}$ being positiv definite, it can also be shown, [BP94], that the condition number of $\tilde{M}_0\tilde{M}$ is uniformly bounded. Therefore the preconditioned conjugate gradient method is used on the system (5) preconditioned by (6).

The temperature distribution is determined by first solving the hyperbolic part of the heat balance equation (2) by the method of characteristics, [DES92], and then solving the elliptic part by the finite element method. The resulting linear system is solved by a preconditioned conjugate gradient method.

DOMAIN DECOMPOSITION

As pointed out earlier, the extrusion problem is rich on localized phenomena, especially near the outlet through the die. The computational domain is divided into overlapping subdomains and refined at locations with large gradients. An example of a domain with a refined area is shown in Figure 2, where a sudden contraction is used to mimic the effect of a die. The pressure-velocity system is elliptic, and can be solved by conventional domain decomposition methods, [CW92], [DW89]. We will be using an additiv Schwarz method.

To illustrate the domain decomposition idea, the classical alternating Schwarz method is used for the heat balance equation. The total computational domain Ω is divided into two subdomains Ω_1 and Ω_2 of equal size and resolution and has a fullsized outlet, see Figure 3. The two subdomains overlap with a given number of elements. The individual boundaries are denoted $\partial\Omega_i$, in which the interior surfaces Γ_i are included, $i = 1, 2$. The initial-boundary value problem for the temperature is stated below, where the vector-valued function $\mathbf{f}$ is a given velocity field, the function g is a boundary function and θ_{t_0} is an initial profile.

$$\begin{array}{rcll} \mathrm{Pe}(\dfrac{\partial\theta}{\partial t} + \mathbf{u}\cdot\nabla\theta) & = & \nabla^2\theta + \beta\epsilon : \tau & \text{in } [0,T]\times\Omega \subset R^3, \\ \mathbf{u}(x,y,z) & = & \mathbf{f}(x,y,z) & \text{in } \Omega, \\ \theta(x,y,z,t) & = & g(x,y,z) & \text{on } \partial\Omega \ \forall t, \\ \theta(x,y,z,0) & = & \theta_{t_0}(x,y,z) & \text{in } \Omega \text{ at } t = 0. \end{array} \tag{9}$$

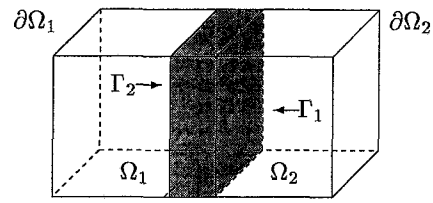

Figure 3 Two equally sized overlapping subdomains.

Before we present the algorithm we introduse some notation. Let $\theta^n_{i,k}$ denote the solution in $\overline{\Omega}_i$ after k Schwarz iterations at timelevel n, and $\theta^n_{2,k}|_{\Gamma_1}$ be the restriction of $\theta^n_{2,k}$ to Γ_1; similarly $\theta^n_{1,k}|_{\Gamma_2}$ is the restriction of $\theta^n_{1,k}$ to Γ_2. The part of the true boundary that surround each of the subdomains except for the interior surface is denoted $\partial\Omega_i\backslash\Gamma_i$, $i = 1, 2$. The characteristic solution at timelevel n is denoted by $\bar{\theta}^n$, and the subscript on the nonlinear part $(\beta\epsilon : \tau)^n_{i,k}$ indicates that the iterate $\theta^n_{i,k}$ is used to linearize. Note that $k = 0$ indicates the characteristic solution.

Algorithm:

1. Solve the hyperbolic part for the characteristic solution $\bar{\theta}^n$:

$$\frac{\partial\theta}{\partial t} + \mathbf{u}\cdot\nabla\theta = 0 \qquad \text{in } \Omega.$$

2. Solve for $\theta^n_{1,1}$:

$$\begin{aligned}
\theta^n_{1,1} &= \frac{\Delta t}{\mathrm{Pe}}\Delta\theta^n_{1,1} + \frac{\Delta t}{\mathrm{Pe}}(\beta\epsilon : \tau)^n_{1,0} + \bar{\theta}^n && \text{in } \Omega_1,\\
\theta^n_{1,1} &= \bar{\theta}^n && \text{on } \Gamma_1,\\
\theta^n_{1,1} &= g && \text{on } \partial\Omega_1\backslash\Gamma_1.
\end{aligned}$$

3. Solve for $\theta^n_{2,1}$:

$$\begin{aligned}
\theta^n_{2,1} &= \frac{\Delta t}{\mathrm{Pe}}\Delta\theta^n_{2,1} + \frac{\Delta t}{\mathrm{Pe}}(\beta\epsilon : \tau)^n_{2,0} + \bar{\theta}^n && \text{in } \Omega_2,\\
\theta^n_{2,1} &= \bar{\theta}^n && \text{on } \Gamma_2,\\
\theta^n_{2,1} &= g && \text{on } \partial\Omega_2\backslash\Gamma_2.
\end{aligned}$$

4. For $k = 2, 3, \ldots$ solve iteratively for $\theta^n_{1,k}$ and $\theta^n_{2,k}$:

$$\begin{cases}
\theta^n_{1,k} = \dfrac{\Delta t}{\mathrm{Pe}}\Delta\theta^n_{1,k} + \dfrac{\Delta t}{\mathrm{Pe}}(\beta\epsilon : \tau)^n_{1,k-1} + \bar{\theta}^n & \text{in } \Omega_1,\\
\theta^n_{1,k} = \bar{\theta}^n_{2,k-1}|_{\Gamma_1}, & \\
\theta^n_{1,k} = g & \text{on } \partial\Omega_1\backslash\Gamma_1,
\end{cases}$$

$$\begin{cases}
\theta^n_{2,k} = \dfrac{\Delta t}{\mathrm{Pe}}\Delta\theta^n_{2,k} + \dfrac{\Delta t}{\mathrm{Pe}}(\beta\epsilon : \tau)^n_{2,k-1} + \bar{\theta}^n & \text{in } \Omega_2,\\
\theta^n_{2,k} = \bar{\theta}^n_{1,k}|_{\Gamma_2}, & \\
\theta^n_{2,k} = g & \text{on } \partial\Omega_2\backslash\Gamma_2.
\end{cases}$$

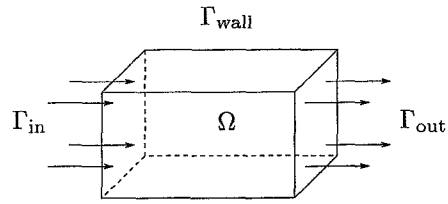

Figure 4 Computational domain, note that $\Gamma_{wall} = \partial\Omega\backslash(\Gamma_{in} \cup \Gamma_{out})$.

NUMERICAL EXAMPLES

In this section we show a solution of the system (2)-(3) for the simple geometry given above.

Consider Ω to be a bounded domain in R^3 with a boundary $\Gamma = \Gamma_{in} \cup \Gamma_{out} \cup \Gamma_{wall}$, i.e. Γ is a union of an in-boundary, an out-boundary and the rest of the total boundary, called the wall-boundary, see Figure (4). In the calculations presented, Γ_{out} is regarded as a free boundary in respect to velocity and temperature.

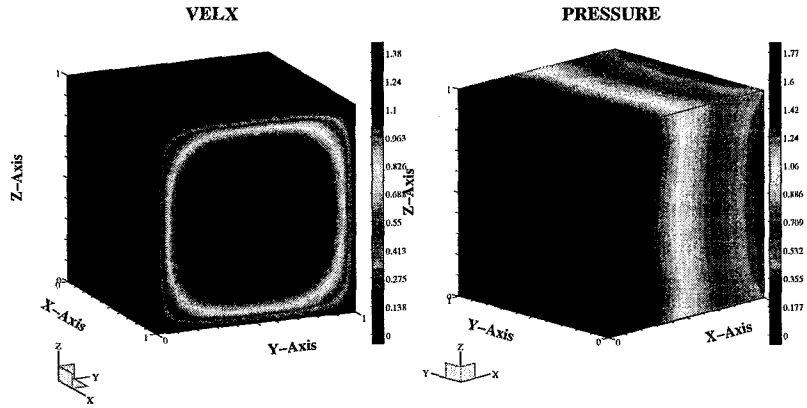

Figure 5 (a) x-component of velocity with a domal profil due to the no-slip condition, and (b) matching pressure with the largest values at Γ_{in} and especially near the corners.

Figure 5 shows the solution to the equations (3) with the boundary conditions

$$\begin{aligned} \mathbf{u} &= [1\ 0\ 0]^t && \text{on } \Gamma_{in}, \\ \mathbf{u} &= \mathbf{0} && \text{on } \Gamma_{wall}, \\ p &= 0 && \text{on } \Gamma_{out}. \end{aligned}$$

The parabolic heat balance equation is solved by the alternating Schwarz method with overlap, following the algorithm discussed above. Results from two different cases are presented. For better to visualize the solutions in the interior of the domain, it is split in two along the flow-direction, and only one half of the domain is shown.

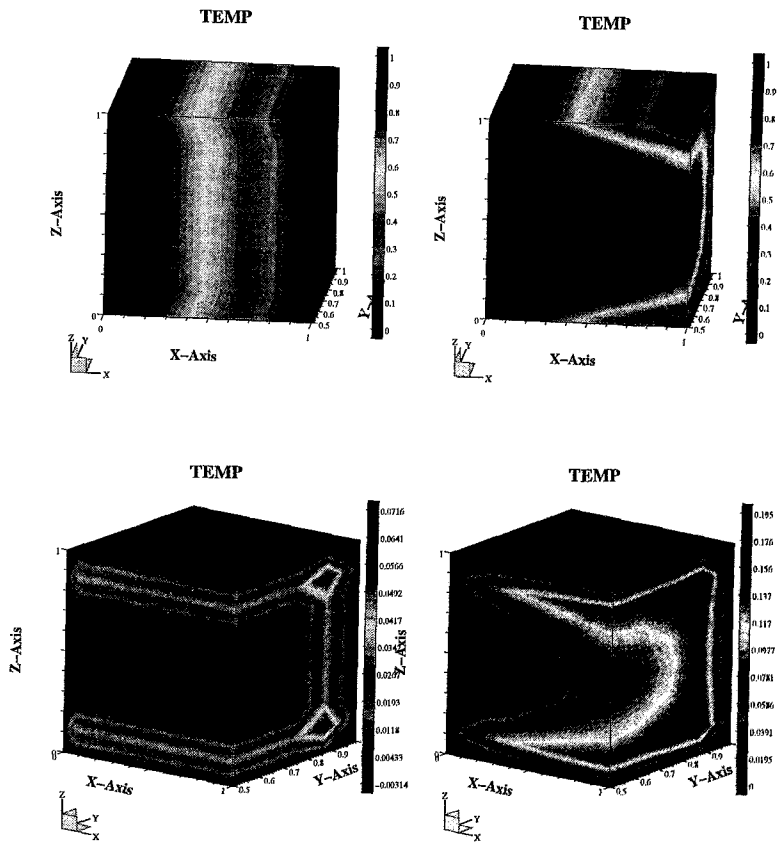

Figure 6 (a) Temperature after 5 timesteps, and (b) after 20 timesteps for the first case. (c) Temperature after 5 timesteps, and (d) after 20 timesteps for the second case.

In Figure 6, (a) and (b), the temperature distribution resulting from solving (9) with

$$\mathbf{f}(x, y, z) = [1\ 0\ 0]^t \qquad \text{in } \overline{\Omega},$$

and linear boundary and initial conditions,

$$\begin{aligned} g(x, y, z) &= 1 - \tfrac{1}{2}x \qquad \text{on } \partial\Omega \backslash \Gamma_{\text{out}}, \\ \theta_{t_0} &= 1 - \tfrac{1}{2}x \qquad \text{in } \Omega, \end{aligned}$$

is shown. In Figure 6, (c) and (d), we have a *no-slip condition causing friction*,

$$\mathbf{f}(x, y, z) = \begin{cases} [1\ 0\ 0]^t & \text{in } \overline{\Omega} \backslash \Gamma_{\text{wall}}, \\ \mathbf{0} & \text{on } \Gamma_{\text{wall}}, \end{cases}$$

and zero conditions on the temperature,

$$\begin{aligned} g(x,y,z) &= 0 \qquad && \text{on } \partial\Omega\backslash\Gamma_{\text{out}}, \\ \theta_{t_0} &= 0 \qquad && \text{in } \Omega. \end{aligned}$$

The main difference between these to cases is due to the no-slip condition in the one case. In the first case the velocity is the same in the hole domain, and the heat is smoothly spreading into the middle of the domain. Looking at a cross section at some point in the flow-direction, the largest values will always be located in the middle. The next case also show smooth spreading into the middle of the domain, but in a cross section similar to the one mentioned above, the largest values will be in the corners and along the edges.

CONCLUSIONS

The tests carried out indicate that the domain decomposition algorithm presented above performs well for the nonlinear parabolic equation compared to the global solution on one domain. The method will, however, be further investigated.
For the nonlinear elliptic pressure-velocity system an additiv Schwarz method gives good results, but further experiments must be (and will be) carried out to support such a statement.

ACKNOWLEDGEMENT

The support provided by Norsk Hydro is gratefully acknowledged.

REFERENCES

[BP94] Bramble J. and Pasciak J. (1994) Iterative techniques for time dependent stokes problems. *Math. Comp.* .

[CW92] Cai X. and Widlund O. (1992) Domain decomposition algorithms for indefinite elliptic problems. *SIAM J. Stat. Comput.* 13: No.1, pp. 243–258.

[DES92] Dahle H., Espedal M., and Sævareid O. (1992) Characteristic local grid refinement for reservoir flow problems. *Int. j. numer. meth. eng.* 34: pp. 1051–1069.

[DW89] Dryja M. and Widlund O. (1989) Towards a unified theory of domain decomposition algorithms for elliptic problems. In *3rd International Symposium on Domain Decomposition Methods for Partial Differential Equations.*

[HSH92] Holthe K., Støren S., and Hansen L. (1992) Numerical simulation of the aluminium extrusion process in a series of press cycles. In *4th International Conference on Numerical Methods in Industrial Forming Processes.*

[Sæv93] Sævareid O. (1993) Simulation of extrusion combining local grid refinement and lagrangian time-marching. In *8th International Conference on Finite Elements in Fluids.*